Unidirectional molecular rotary motor with remotely-switchable rotation direction

Kamil Szychta[1,2] and Joanna Jankowska[2,*]

[1]Faculty of Physics, University of Warsaw, Warsaw 02-093, Poland
[2]Faculty of Chemistry, University of Warsaw, Warsaw 02-093, Poland
[*]Corresponding author, e-mail: jjankowska@chem.uw.edu.pl

Abstract: Light-driven rotary motors allow direct transformation of light energy into unidirectional rotary motion at the nanoscale, giving rise to countless emerging applications in molecular engineering. The key feature enabling the unidirectional rotation and controlling its direction is the motor chirality, an inherently chemical factor, hard to modify postsynthetically. Here we propose a new molecular rotary motor architecture, **E-motor**, in which the motor operation direction can be switched *in situ*, without the need for chemical modification of the system structure. This effect is achieved by application of an external electric-field pulse, and is intended to provide means for chirality control in motors deposited on a surface. Our study relies on quantum-chemical calculations and nonadiabatic molecular dynamics simulations performed for a specifically-tailored system, PFCN, designed to provide illustration for the proposed new motor type. We show that the model system's chirality and, hence, its operation direction, depends on orientation of a covalently bound polar switching unit, which can be controlled with an external electric field. At the same time, the proposed system manifests all characteristic photophysical properties of a unidirectional molecular motor, and its set chirality is preserved, i.e., it is thermally and optically stable during the regular motor operation in the absence of the electric field.

Introduction

Molecular rotary motors belong to a growing family of functional molecular devices capable of transforming chemical, electric, or light energy into mechanical work,[1–3] offering unprecedented means for controlling motion at the nanoscale and opening way for design of interactive, 'smart' molecular systems and materials for countless applications.[4–14] Among other molecular systems of such kind, often referred to as molecular machines,[2,5,15–17] light-driven rotary motors characterize with continues unidirectional rotary motion under a flux of photons of energy matching the electronic absorption spectrum of the motor. In the course of this motion, a part of molecular system considered static, the 'stator', constitutes a reference framework for the other, mobile part,

the 'rotor', and the unidirectionality of the rotation stems from the inherent system chirality. The historically first and the nowadays most populated group of molecular motors are overcrowded alkenes, in which the light-triggered rotation occurs about a double C=C bond. It is important to note that, amid the overcrowded alkenes, three generations of motors can be distinguished:[18] (i) the first-generation, in which stationary and rotating parts of the molecule are identical, both possessing same-oriented stereogenic centres, (ii) the second-generation, in which two halves of the motor are different and both, or only one of them, possess a stereogenic centre, and (iii) the third-generation, in which, contrary to the previous two, the motor consists of one pseudo-chiral stator and two rotors, bonded on its opposite sites.

From the perspective of this work, the axial chirality of molecular rotary motors, i.e., their preference for adopting one of the two possible relative orientations of the rotating and stationary parts, plays an essential role. The motor chirality enables the unidirectional rotation and controls its direction.[15] The origin of this effect lies, on the one hand, in the presence of a point stereogenic centre (chiral or pseudo-chiral) and, on the other, in the sterically crowded surrounding of the central double bond about which the rotation occurs. Due to fundamentally chemical nature of the both factors, artificial motors' chirality and resulting rotation direction can be controlled almost exclusively at the synthesis stage, usually through separation of enantiomers from a racemic mixture of the synthesised product,[18] or by taking advantage of the asymmetric synthesis routes.[19,20] At the same time, over the years, several attempts to reverse the rotation direction of a once prepared optically-driven motor have been made. Firstly, the circularly-polarized light was utilized to control motion of an inherently non-chiral molecular rotor,[21] however, the overall prevalence of one direction of rotation over the other did not exceed 1%. Alternatively, post-synthetic base-catalyzed epimerization,[22] and achiral-host – chiral guest noncovalent interactions[23] were used to switch between clockwise / counterclockwise motor operation. A similar, catalytic strategy has been also recently employed to control rotation about a single bond in a chemically-powered molecular rotor.[24] The latter approaches, though, all involve a full-scale chemical intervention. Eventually, a robust, real-time control of rotation in molecular motors still remains a major challenge.[25]

In the present work, we propose a new kind of molecular rotary motor whose direction of rotation can be controlled post-synthetically and on demand, by an external electric-field switching pulse. The designed system and its working principle have been formulated on the grounds of quantum-chemical and nonadiabatic molecular dynamics simulations. Our conceptual starting point is the second-generation motor structure which we redesign by transfering the point stereogenic centre to a rotating, switchable unit eventually achieving the motor's axial chirality dependence on the orientation of the newly-added switch (Figure 1). The proposed switch is electric-field sensitive: it characterizes with a large electric dipole moment, allowing for its orientation to be controlled with an external electric field. At the same time, thanks to optimized steric repulsion between the switch and the principal framework of the motor, after the switch orientation is set with the electric-field pulse, it is thermally (and optically) stable. Eventually, the motor can undergo a unidirectional, optically-driven rotation in the absence of the field. It should be stressed that the discussed effect requires control of the motor orientation with respect to the external electric-field

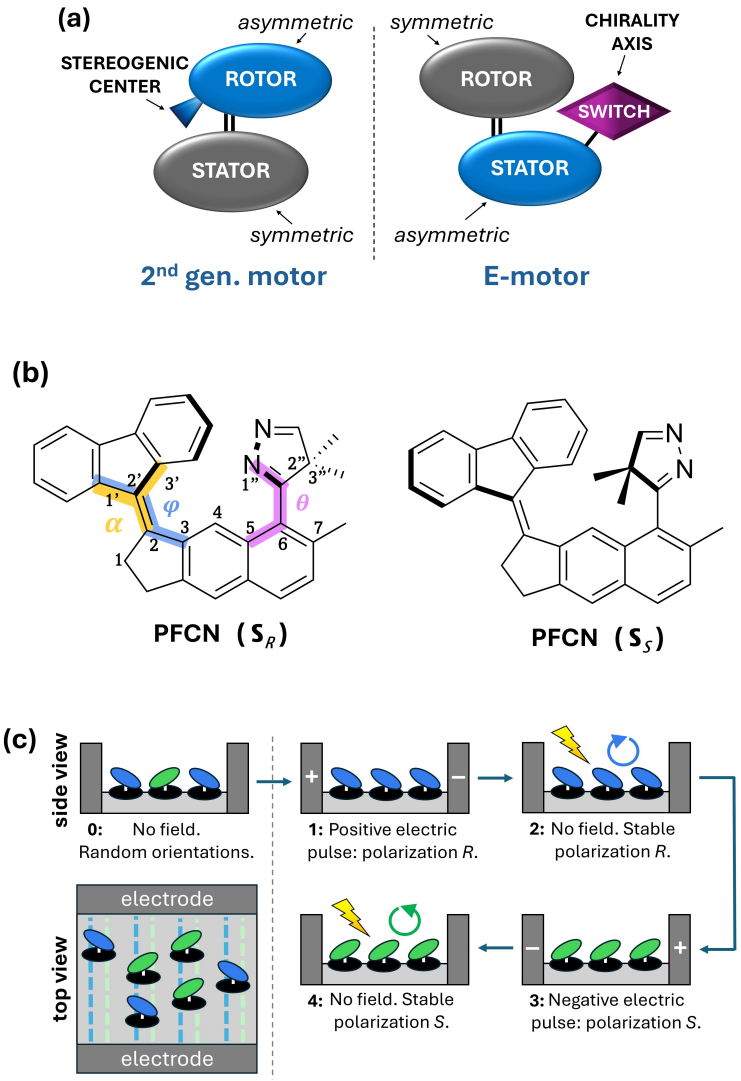

Figure 1: **Electric-field switchable motor structure.** **(a)** Functional structure comparison between a typical second-generation motor and the switchable **E-motor** proposed in this work. **(b)** Chemical structure of the investigated PFCN system representing the **E-motor** class in its two stable chirality forms: $\mathbf{S}_R$ and $\mathbf{S}_S$. The three marked dihedral angles allow to track key structural changes of the operating motor: $\varphi \equiv \measuredangle$ 1'-2'-2-3 (rotation of the rotor, in blue), $\theta \equiv \measuredangle$ 1"-2"-6-7 (rotation of the switch, in purple), $\alpha \equiv \measuredangle$ 2'-1'-3'-2 (rotor pyramidalization, in yellow). **(c)** Working principle and proposed arrangement of an array of electric-field controlled molecular rotary motors.

source, thus, it is suited for controlling chirality of motors deposited on a surface.[26–29] To assure all-R or all-S chirality of a manifold of motors, their stator components need to be aligned, e.g. in a way proposed in Figure 1 (c), which can be achieved by proper functionalization of the surface by chemical or photolithographical means.[30–35]

Results and discussion

Detailed structure description of the PFCN motor

To illustrate the proposed new motor-design with a specific chemical realization, in this work we investigate by means of quantum-chemical methods a (9E)-9-(13-Methyltricyclo[7.4.0.0^{3,7}]trideca-1,8,10,12-tetraen-4-ylidene)-4b,8a-dihydro-9H-fluorene molecule (PFCN), whose chemical structure has been shown in Figure 1. The proposed motor is composed of three distinguishable parts: (i) a symmetric rotor, (ii) an asymmetric stator, and (iii) a polar switching unit.

The employed rotor is made of a flat fluorene moiety, often used as a stationary unit in the second-generation motors.[15,27,36] It characterizes with a C_{2v} symmetry and, hence, its rotation by 180° leaves the system unchanged from a chemical point of view. Eventually, for a fixed-chirality operation cycle, the proposed motor is bistable, in similarity to its second-generation parent. Furthermore, the rotating-fragment high symmetry assures it does not contribute to the total-system electric dipole moment.

The chosen stator, specifically its indane part, also resembles the rotating component popularly used in the first- and second-generation motors.[18,37] The key difference is the lack of a methyl group at the cyclopentene ring which, in traditional chiral motors, gives origin to the point stereogenic center. Another difference is addition of an extra toluene ring at the other side of the stator. This added fragment provides a scaffold for the switching unit. What should be noted is also an important role of the end methyl group within the toluene fragment which protects the thermally-activated switch from undesired rotation about the single C–C bond in the absence of electric field.

Finally, the new motor component, the switching unit, is added at the far end of the stator. In the studied system, it is composed of a five-member, pyrazole-like ring with a dimethyl substituent placed opposed to nitrogen atoms. Eventually, one arrives with a push-pull moiety characterized with a pronounced dipole moment, with the negative charge localizing at the nitrogens, and the positive charge localizing at the methyl side of the switch. Importantly, the steric bulkiness of the switching unit is also strongly asymmetric. Thus, after the switch adopts its most energetically-favourable perpendicular orientation with respect to the stator plane, its interaction with the rotor gives rise to a preference for one of the two axially-chiral isomers (S or R), depending on the switch orientation. Interestingly, also the switch orientation by itself can be described in terms of axial chirality. This puts the here-proposed **E-motor** into contrast with the motor architectures known so far, in which the operation direction is controlled either by a point stereogenic center (first- and second-generation motors), or by a pseudo-stereogenic structural arrangement (third-generation

motors), with a noticeable exception of the achiral-host – chiral guest switchable molecular rotor mentioned earlier.[23]

Ground-state characterization of PFCN stable and metastable forms in the absence of electric field

Below, and in the following section, to investigate the PFCN properties, we apply a recently developed multi-reference semi-empirical method, ODM2/MRCI-SD,[38] which allows for a robust, fully quantum-chemical treatment of the designed system's electronic structure, both in the ground and in the excited electronic states. All technical details regarding the performed calculations can be found in the Supporting Information (SI) accompanying this publication.

Firstly, it should be pointed out that, in the ground electronic state, two mirror pairs of stable, **S**, and metastable, **M**, structures can be optimized: one pair for the *R* (clockwise), and another for the *S* (counterclockwise) motor rotation direction, as illustrated in Figure 2. It is also worth to note that the operation chirality of the motor is governed by the chirality of its **S** form, while the chirality of the **M** isomer participating in a given rotation cycle is always opposite. Upon a look at the optimized **S** and **M** structures and their characteristic features depicted in Figure 2, one can immediately see the energy equivalence between the **S** and **M** forms of different chirality: an anticipated effect, given the chemical identity of these species. The ground-state relative energy of the metastable form is found at about 170 meV (3.9 kcal/mol), which resembles values reported for some known motors,[39–42] and which assures thermodynamic equilibrium to be quantitatively shifted towards the stable isomer under the room-temperature conditions.

Structure-wise, the key difference between the **S** and **M** isomers is the extent of the out-of-plane displacement of the rotor with respect to the stator, measured with dihedral angle φ, defined in Figure 1. In the absence of steric hindrance, this angle should be close to 0°/180° which would correspond to a flat arrangement, energetically preferred in the C=C bonded sp^2 systems. At the same time, due to the steric repulsion between the rotor and the switching unit, this angle becomes distorted from planarity. Depending on which side of the switch the rotor moiety is interacting with, the repulsion strength varies, giving rise to different energies and different φ values of the **S** and **M** forms. Importantly, this varying repulsion does not induce pronounced changes in the orientation of the switching unit, measured with dihedral angle θ, also defined in Figure 1.

The key electric and UV-Vis absorption properties of PFCN are shown in Table 1 on the example of the $\mathbf{S}_R$ and $\mathbf{M}_S$ forms. Firstly, one should notice a pronounced ground-state electric dipole moment of both isomers which is, to most extent, preserved upon excitation to the two lowest-energy singlet excited states, S_1 and S_2. It should be also noted that, in both forms, the S_1 state is the bright state which can be reached with the UV light irradiation of about 3.75 eV (330 nm), and whose electronic configuration differs from a closed-shell ground-state configuration predominantly by the HOMO → LUMO electron excitation. On the contrary, the S_2 state, which requires excitation energy of roughly 4.20 eV (295 nm), shows dominant HOMO-1 → LUMO excitation character and negligible oscillator strength. Upon inspection of the relevant orbital

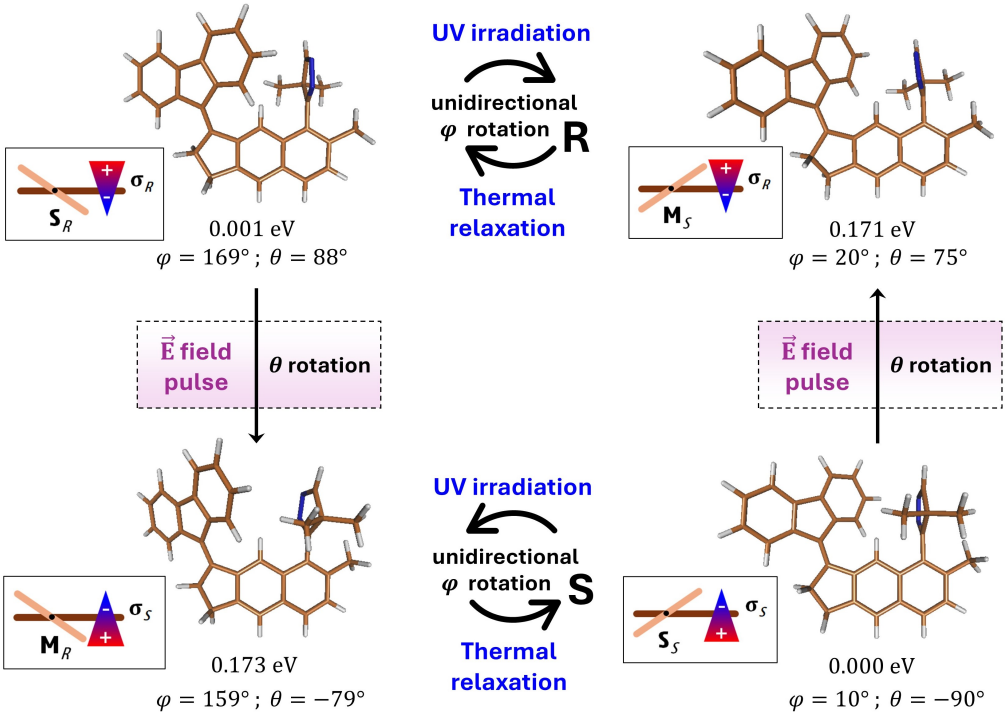

Figure 2: **Operation cycle and switching scheme of PFCN.** Displayed structures correspond to the ground-state stable PFCN forms, with indicated relative energies and characteristic dihedral angles, φ and θ, as defined in Fig. 1. The chirality of the motor forms (**S**/**M**) and the switching unit ($\boldsymbol{\sigma}$) has been indicated in the inset pictures.

plots shown in the SI (Section 1), it can be concluded that the S_1 state follows the typical pattern known for unsubstituted overcrowded-alkene motors, in which the lowest excited state is strongly delocalized, with clear $\pi\pi^*$ character, and in which the initially double C=C bond between the rotor and the stator acquires a single-bond nature. The S_2 state, on the other hand, has a strong rotor-to-stator charge-transfer character, which is likely responsible for the low $S_0 \rightarrow S_2$ absorption intensity. Above-discussed PFCN key ground-state and UV-Vis absorption features have been confirmed also at the ab initio level of theory: results of these calculations can be found in a dedicated Section 2 in the SI.

Potential energy landscape of a full PFCN rotation cycle

As has been already indicated, the most straightforward comparison of the new motor's predicted operation mechanism can be made to that of the second-generation motors. Namely, for a given rotation chirality set by the orientation of the switch, the system starts with an optical $S_0 \rightarrow S_1$ excitation of its stable isomer, **S**, initiating so-called 'optical' step of the rotation cycle. From that moment, PFCN structure begins to evolve at the first excited-state potential energy surface (PES), which can be followed with the reaction path profile shown in Figure 3 (a). Thanks to the maintained overcrowded-alkene character, PFCN is expected to adiabatically relax on the S_1

Table 1: UV-Vis absorption properties of the $\mathbf{S}_R$ (**S**) and $\mathbf{S}_R$ (**M**) isomers, determined at the ODM2/MRCI-SD level of theory.

S	E_{ex} (eV)	f	El. config.	$\lvert\mu\rvert$ (Debye)
S_0	—	—	—	4.65
S_1	3.770	0.4641	H–L (91%)	4.20
S_2	4.169	0.0052	H-1–L (85%)	5.81
M	E_{ex} (eV)	f	El. config.	$\lvert\mu\rvert$ (Debye)
S_0	—	—	—	4.38
S_1	3.765	0.2611	H–L (91%)	4.28
S_2	4.204	0.0034	H-1–L (84%)	5.31

E_{ex} – $S_0 \rightarrow S_x$ excitation energy; f – transition oscillator strength; El. config. – dominant orbital contributions to the electronic transition; $|\mu|$ - state electric dipole moment.

PES from the **S** Franck-Condon region towards the area of small S_1/S_0 energy-gap values, where the central C=C bond between the rotor and the stator adopts close-to-perpendicular orientations. Two similar, yet unequal minimum-energy conical intersections (MECIs) have been found along this route, marked in Figure 3 (a) as $\mathbf{MECI_{out}}$ and $\mathbf{MECI_{in}}$. Both characterize with perpendicular rotor orientation and strong pyramidalization of the top carbon atom participating in the C=C bond, but differ in the direction of this pyramidalization, with $\mathbf{MECI_{in}}$ showing slightly lower adiabatic energy of 3.041 eV vs. 3.120 eV for $\mathbf{MECI_{out}}$. Both these energies lie well below the initial $S_0 \rightarrow S_1$ excitation energy, making the identified MECIs energy-accessible. Eventually, it can be expected that, once the system arrives in their vicinity, efficient relaxation to the ground electronic state should take place, similarly as in the second-generation motors.[43–45] After landing on the S_0 PES, the motor can either come back to the starting **S** isomer, or continue rotation towards the **M** form (right panel of Figure 3 (b)). In the latter case, the vibrationally hot system encounters only minimal energy barrier of about 110 meV (2.5 kcal/mol) to complete the final, so called 'thermal' step of the rotation cycle, reaching the product **S** form, chemically equivalent to the starting point. The expected, only short-time population of the metastable form shows some resemblance of the PFCN operation cycle to that of the two-stroke second-generation motor proposed recently by Olivucci et al.[46]

Having said all this, we would like to draw the reader's attention back to the problem of the system chirality. The reaction path shown in Figure 3 (a) and in the right panel of Figure 3 (b) illustrates the clockwise rotation of PFCN, sequentially populating the $\mathbf{S}_R \rightarrow \mathbf{M}_S \rightarrow \mathbf{S}_R$ structures. To reverse the motor rotation direction, one would need to reverse the chirality of the **S** isomer. Having in mind that the **S** and **M** forms participating in the same rotation cycle characterize with the opposite chirality, this problem is equivalent to reversing the relative stability of these forms. This effect can be achieved through rotation of the PFCN switching unit, i.e., through its axial chirality inversion, as illustrated in the central panel of Figure 3 (b). Upon such rotation, the $\mathbf{S}_R$ isomer transforms into $\mathbf{M}_R$ which is then expected to undergo quick thermal relaxation to form the $\mathbf{S}_S$ structure. Once formed, $\mathbf{S}_S$ can participate in the reversed chirality, i.e., in the *S*-chirality motor operation cycle whose ground-state potential energy landscape, shown in the left panel of Figure 3 (b), mirrors that of the *R*-rotation, discussed previously. Importantly, in the absence of an external potential, the switching unit rotation requires substantial amount of

energy: about 680 meV (15.7 kcal/mol). This value is about 25% smaller than the energy barrier protecting the system from the ground-state **S** → **M** forward rotation, corresponding to the tall peaks in Figure 3 (b): 918 meV, equivalent to 21.2 kcal/mol. Eventually, spontaneous reversal of the motor's chirality appears unlikely, which assures unidirectionality of the PFCN motor operation once the switch position is set. Nevertheless, it should be pointed out that the modular structure of the proposed **E-motor** allows for almost independent control of the switch rotation barrier with chemical substitution at site 7 (Figure 1), allowing its adjustment to one's individual needs, as has been illustrated with few examples in the SI (Section 3).

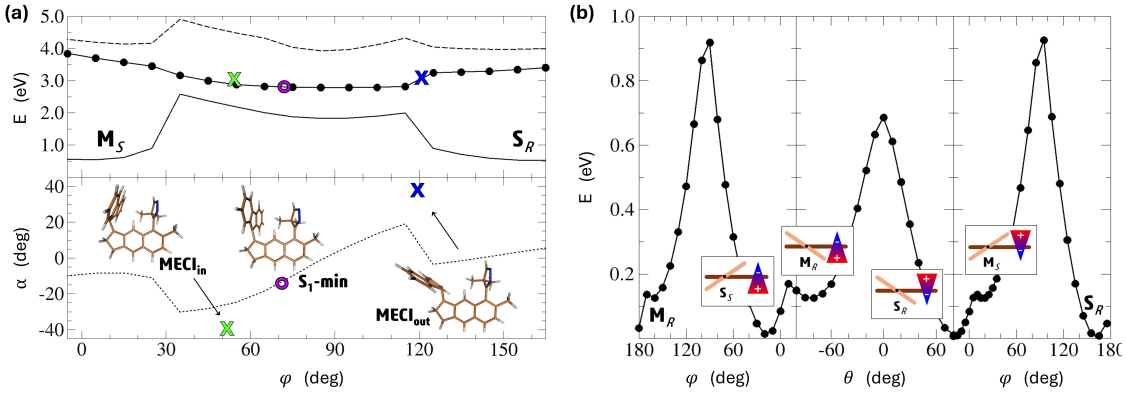

Figure 3: **Potential energy profiles along the rotor (φ) and the switch (θ) rotation coordinates calculated in the absence of the electric field.** **(a)** Rotor rotation during the optical step. Upper panel: energies calculated at PFCN structures optimized in the S_1 state (solid line – S_0, full circles – S_1, dashed line – S_2). The **X**-signes show positions of the optimized minimum-energy conical intersections, and the purple circle marks the optimized S_1 minimum. Lower panel: Correlation between the rotor pyramidalization (α) and rotation dihedral angles (φ) along the optimized S_1-profile, and at identified key structures. **(b)** Ground-state potential energy profiles calculated along the rotor rotation coordinate (side panels), and for the PFCN chirality switching (central panel). The left and right panels correspond respectively to the S and R motor rotation cycles.

Electric-field control of the motor chirality

The large PFCN dipole moment originates primarily from presence of the strongly-polarized switching unit, whose electronic structure is shaped by push-pull effects induced by the dinitrogen and dimethyl substituents. Eventually, the total dipole moment aligns almost perfectly with the direction of the switch, which opens possibility for its manipulation with an external electric potential.

In this respect, a simple picture of an electric dipole, $\vec{\mu}$, undergoing reorientation in the presence of an electric field, $\vec{E}$, might provide a good conceptual starting point. With the general expression for the dipole's energy under field conditions, $E = -\vec{\mu} \cdot \vec{E}$, and given the perpendicular orientation of the switch in both PFCN stable forms, **S** and **M**, one can expect that the energy of one of the forms should increase while the other's should decrease upon application of an electric field in a direction perpendicular to the stator plane. At the same time, the absolute potential energy at the maximum of the switch rotation barrier (middle panel of Figure 3 (b)) should not change much, as

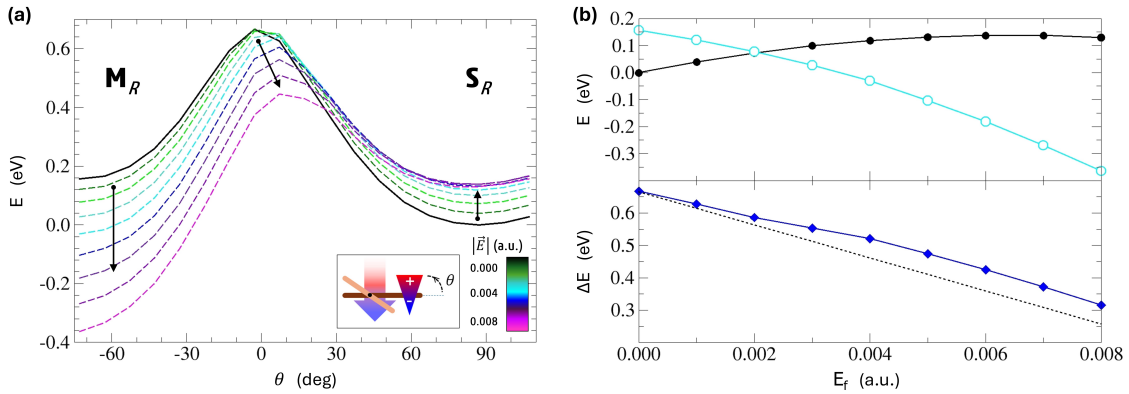

Figure 4: **Electric field impact on PFCN key-form energies in the ground electronic state. (a)** Adiabatic potential energy profiles calculated between the $\mathbf{S}_R$ and $\mathbf{M}_R$ forms along the switch-rotation coordinate at varying electric field intensities. **(b)** Extracted energies of the $\mathbf{S}_R$ (black full circles) and $\mathbf{M}_R$ (empty cyan circles) isomers (top panel), and of $\mathbf{S}_R \rightarrow \mathbf{M}_R$ switching barriers (blue diamonds), along with the linear electric-field stabilization function predicted with the dipole model (dotted black line) (bottom panel).

this point corresponds to the null value of the $\vec{\mu} \cdot \vec{E}$ scalar product. Eventually, one can not only manipulate the PFCN isomer energies, but also control the relative energy barrier for the switch rotation, i.e., the amount of energy necessary to reverse the motor operation direction.

In Figure 4 (left panel), we show potential energy profiles for the switching-unit rotation in the presence of the external electric field of varying magnitude, calculated at the Density Functional Theory level (methodological details of these calculations are disclosed in Section 1 in the SI). In the studied case, the field is oriented perpendicularly to the stator, and its direction has been chosen so as it stabilizes the $\mathbf{M}_R$ isomer, and destabilizes the $\mathbf{S}_R$ motor form. In the right panel of Figure 4, key energy values associated with the switch rotation have been extracted, for an easier reference.

First and foremost, upon inspection of Figure 4, it can be noticed that expected changes of the key motor-forms' energies formulated on the grounds of the simple dipole model are confirmed. With the increasing field strength, one can observe continues lowering of the $\mathbf{M}_R$ energy, while the $\mathbf{S}_R$ energy undergoes a noticeable rise, which leads to intended reversal of the $\mathbf{S}$ and $\mathbf{M}$ forms stability. Importantly, these changes are accompanied with a monotonic decrease of the $\mathbf{S} \rightarrow \mathbf{M}$ energy barrier. Eventually, when the barrier drops to the level comparable to thermal energy available to the system, a spontaneous $\mathbf{S}_R \rightarrow \mathbf{M}_R \rightarrow \mathbf{S}_S$ transformation is anticipated, realized through the switching-unit rotation followed by a thermal rotor relaxation.

Upon a closer look at data shown in Figure 4, one can notice that, while the observed changes' trends follow the expectations, their quantitative evolution with increasing field strength diverges from the linear behavior predicted on the grounds of the dipole model. First of all, after initial destabilization under the weak electric field, the $\mathbf{S}$ form energy ceases to increase for field intensities greater than 0.005 a.u. Secondly, while for weaker fields the energy maximum along the switch

rotation path does not undergo noticeable changes, at $|\vec{E}|$ of about 0.004 a.u. lowering of the barrier starts to be observed. These findings indicate that, at intensity of about 0.004-0.005 a.u., the electric field becomes strong enough to make the higher-order electric effects (such as molecular polarizability) dominate over the linear (dipole) effect in the investigated PFCN system. Nevertheless, the resulting combination of effects leads to promotion of the desired electric-field induced chirality inversion. Finally, it should also be underlined that the investigated electric-field intensity range falls well within technical capabilities of dedicated equipment used, e.g., in electro-catalytic studies.[47] In terms of the required voltage, the 0.008 a.u. electric field intensity corresponds to roughly 4 V/nm. Hence, switching a single layer of motors resembling the PFCN properties could be technically rendered possible already with a scanning tunneling microscope (STM) setup.[48–50]

Real-time simulations of the PFCN motor performance

Finally, to ultimately confirm the molecular rotary motor character of the proposed PFCN system, we have performed nonadiabatic molecular dynamics (NAMD) simulations for the photoexcited $\mathbf{S}_R$ form relaxation, details of which have been described more extensively in the SI (Section 4). In the course of the simulations, an ultrafast, single-exponential decay of the excited-state population has been observed (Figure 5 (a)), with fitted half-lifetime of about 3.6 ps, which stays in line with timescales observed in some second-generation motors.[44,51] Analysis of $S_1 \rightarrow S_0$ relaxation points (Figure 5 (b)) revealed that the leading deactivation mechanism involves funneling through the lower-energy, $\mathbf{MECI_{in}}$ conical intersection. In addition, some more extended relaxation area has been also observed between $\mathbf{MECI_{in}}$ and $\mathbf{MECI_{out}}$, corresponding to central, low energy-gap S_1 PES region identified previously along the optical-step motor reaction path (Figure 3).

To have a notion of the temporal system evolution along the predicted reaction paths, in Figure 5 (c and d) we have also shown kernel density plots for the two PFCN characteristic dihedral angles: φ, and θ. Focusing on the rotor evolution first (Figure 5 (c)), one can observe that the initial, well-concentrated distribution centred around the $\mathbf{S}_R$-optimized φ value consistently evolves towards perpendicular rotor/stator orientation. After reaching this region, about half of the simulated NAMD trajectories successfully relaxes to the ground electronic state within the time-span of the performed simulations. After the relaxation, trajectories split into two packets: one, continuing rotation towards the $\mathbf{M}_S$ form, and another, returning to the starting $\mathbf{S}_R$ structure, which stays in agreement with the known behavior of molecular-motor systems. Quantitatively, in our simulations 34 out of 60 trajectories that relaxed to the S_0 state continued the R-direction rotation. Interestingly, 11 of them managed to go even further, beyond the metastable isomer, overcoming the thermal barrier to form the rotated $\mathbf{S}_R$ isomer.

Concluding analysis, essential for assessing PFCN eligibility to act as a switchable unidirectional rotary motor, is checking the switching unit stability in the course the optical motor operation. This can be done by looking at the switch direction changes in the course of the photodynamics simulations. Upon inspection of Figure 5 (d), one can immediately spot a well-picked distribution of initial θ values, confirming the R chirality of the starting stable isomer. As the dynamics proceeds towards the $S_1 \rightarrow S_0$ relaxation region on the S_1 PES, gentle broadening of this peak is

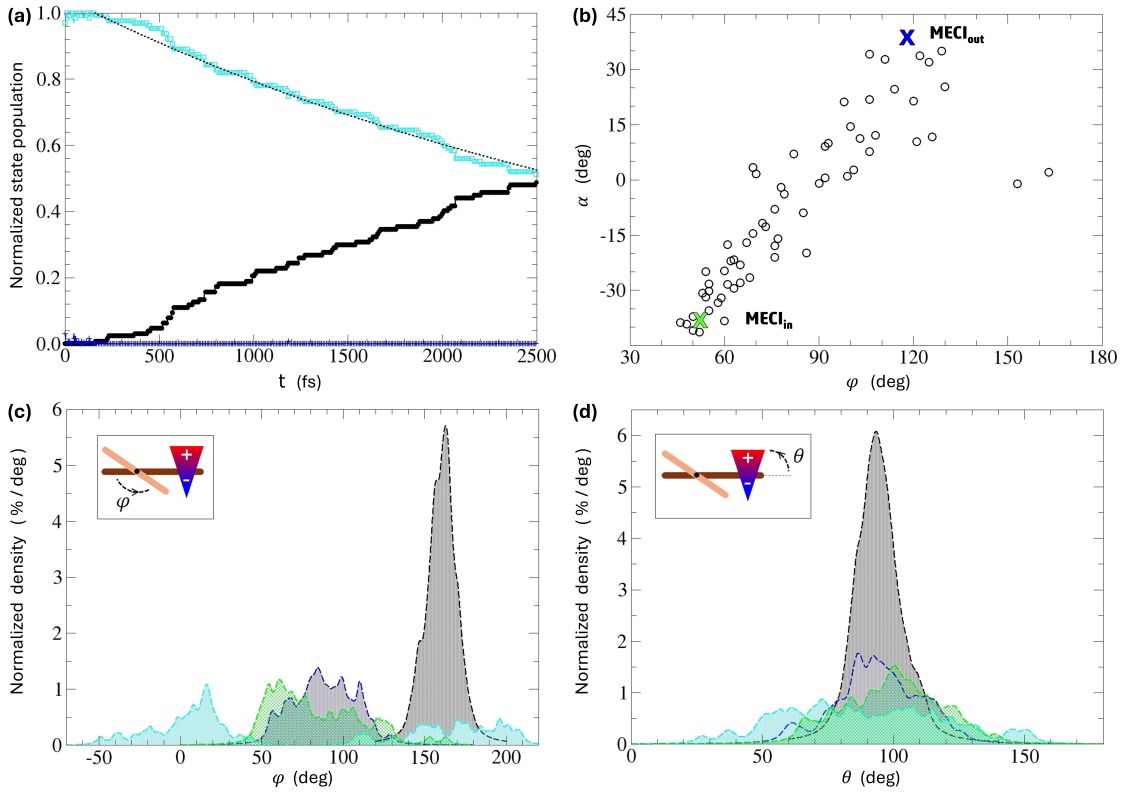

Figure 5: **Nonadiabatic molecular dynamics simulations of the PFCN motor operation.** **(a)** Normalized mean electronic-state populations evolution in NAMD: black full circles – S_0, empty cyan squares – S_1, blue crosses – S_2, black dotted line – exponential fit to the mean S_1 population decay. **(b)** φ/α dihedral angle correlation plot at $S_1 \rightarrow S_0$ hopping points in NAMD simulations. The green and blue crosses mark positions of the optimized minimum-energy conical intersections; Kernel density plots for φ **(c)** and θ **(d)** dihedral angles in the NAMD simulations. Black – initial distribution, green – distribution at $S_1 \rightarrow S_0$ hopping points, cyan – final distribution from relaxed trajectories (finished in the S_0 state), and blue – final distribution from unrelaxed trajectories (finished in the S_1 state).

observed. After the relaxation, this effect becomes even more pronounced, which can be ascribed to increasing kinetic energy accumulated in the system. At the same time, the span of dihedral angles visited by the switching unit in the course of the dynamics never comes near a point at which its orientation could be flipped, which would result in the instability of system's chirality. Eventually, we conclude on promising PFCN properties for application as an electric-field switchable molecular rotary motor.

Conclusions

In this contribution, we have proposed a new molecular rotary motor architecture in which, for the first time, the motor operation direction can be switched *in situ*, without the need for chemical modification of the system structure. This is achieved by application of an external electric-field pulse, and is intended to control chirality of motors deposited on a surface. Our study relies on quantum-chemical calculations and nonadiabatic molecular dynamics simulations performed for a specific chemical system, PFCN, designed to provide illustration for the proposed new motor type. On the grounds of the obtained results, we show that the model system's chirality and, hence, its operation direction, depends on axial chirality of a covalently bound polar switching-unit, which can be efficiently controlled with an external electric field. At the same time, the proposed system manifests all characteristic photo-physical properties of a unidirectional molecular motor, and its chirality is preserved, i.e., it is thermally and optically stable during the regular motor operation in the absence of the field.

Acknowledgements

We gratefully acknowledge Polish high-performance computing infrastructure PLGrid (HPC Center: ACK Cyfronet AGH) for providing computer facilities and support within computational grant no. PLG/2023/016751. K.Sz. thanks Dr. Davide Accomasso of the University of Warsaw for his advice and training on the MRSF-TDDFT calculations. J.J is grateful to Dr. Arkadiusz Trawiński, and to Dr. Wojciech Danowski and Prof. Michał Tomza from the University of Warsaw for fruitful discussions on the manuscript.

Online content

All employed methods description, additional references, source data, supplementary information, details of author contributions, and of competing interests are available at https://doi.org/nnnnn.

References

[1] Mondal, A., Toyoda, R., Costil, R. & Feringa, B. L. Chemically Driven Rotatory Molecular Machines. *Angewandte Chemie International Edition* **61**, e202206631 (2022).

[2] Corra, S., Curcio, M. & Credi, A. Photoactivated Artificial Molecular Motors. *JACS Au* **3**, 1301–1313 (2023).

[3] Srivastava, G. *et al.* Driving a Third Generation Molecular Motor with Electrons Across a Surface. *ACS Nano* **17**, 3931–3938 (2023).

[4] Krause, S. & Feringa, B. L. Towards artificial molecular factories from framework-embedded molecular machines. *Nature Reviews Chemistry* **4**, 550–562 (2020).

[5] Deng, Y. *et al.* Photo-responsive functional materials based on light-driven molecular motors. *Light: Science & Applications* **13**, 63 (2024).

[6] van Dijk, L. *et al.* Molecular machines for catalysis. *Nature Reviews Chemistry* **2**, 0117 (2018).

[7] Gallagher, J. M., Roberts, B. M., Borsley, S. & Leigh, D. A. Conformational selection accelerates catalysis by an organocatalytic molecular motor. *Chem* **10**, 855–866 (2024).

[8] Chen, S. *et al.* Photoactuating Artificial Muscles of Motor Amphiphiles as an Extracellular Matrix Mimetic Scaffold for Mesenchymal Stem Cells. *Journal of the American Chemical Society* **144**, 3543–3553 (2022).

[9] Johnson, T. G. & Langton, M. J. Molecular Machines For The Control Of Transmembrane Transport. *Journal of the American Chemical Society* **145**, 27167–27184 (2023).

[10] Andreoni, L. *et al.* Photochemical Energy Conversion with Artificial Molecular Machines. *Energy & Fuels* **35**, 18900–18914 (2021).

[11] Guinart, A. *et al.* Synthetic molecular motor activates drug delivery from polymersomes. *Proceedings of the National Academy of Sciences* **120**, 2017 (2023).

[12] Siti, W. *et al.* Autonomous DNA molecular motor tailor-designed to navigate DNA origami surface for fast complex motion and advanced nanorobotics. *Science Advances* **9** (2023).

[13] Corra, S., Curcio, M., Baroncini, M., Silvi, S. & Credi, A. Photoactivated Artificial Molecular Machines that Can Perform Tasks. *Advanced Materials* **32**, 1–22 (2020).

[14] Aprahamian, I. The Future of Molecular Machines. *ACS Central Science* **6**, 347–358 (2020).

[15] Sheng, J., Pooler, D. R. & Feringa, B. L. Enlightening dynamic functions in molecular systems by intrinsically chiral light-driven molecular motors. *Chemical Society Reviews* **52**, 5875–5891 (2023).

[16] Zhang, L. *et al.* An electric molecular motor. *Nature* **613**, 280–286 (2023).

[17] Zwick, P., Troncossi, A., Borsley, S., Vitorica-Yrezabal, I. J. & Leigh, D. A. Stepwise Operation of a Molecular Rotary Motor Driven by an Appel Reaction. *Journal of the American Chemical Society* **146**, 4467–4472 (2024).

[18] Pooler, D. R. S., Lubbe, A. S., Crespi, S. & Feringa, B. L. Designing light-driven rotary molecular motors. *Chemical Science* **12**, 14964–14986 (2021).

[19] Neubauer, T. M. *et al.* Asymmetric synthesis of first generation molecular motors. *Organic Letters* **16**, 4220–4223 (2014).

[20] van Leeuwen, T., Danowski, W., Otten, E., Wezenberg, S. J. & Feringa, B. L. Asymmetric Synthesis of Second-Generation Light-Driven Molecular Motors. *The Journal of Organic Chemistry* **82**, 5027–5033 (2017).

[21] Huck, N. P. M., Jager, W. F., de Lange, B. & Feringa, B. L. Dynamic control and amplification of molecular chirality by circular polarized light. *Science* **273**, 1686–1688 (1996).

[22] Ruangsupapichat, N., Pollard, M. M., Harutyunyan, S. R. & Feringa, B. L. Reversing the direction in a light-driven rotary molecular motor. *Nature Chemistry* **3**, 53–60 (2011).

[23] Wezenberg, S. J. & Feringa, B. L. Supramolecularly directed rotary motion in a photoresponsive receptor. *Nature Communications* **9**, 1984 (2018).

[24] Borsley, S., Kreidt, E., Leigh, D. A. & Roberts, B. M. W. Autonomous fuelled directional rotation about a covalent single bond. *Nature* **604**, 80–85 (2022).

[25] García-López, V., Liu, D. & Tour, J. M. Light-Activated Organic Molecular Motors and Their Applications. *Chemical Reviews* **120**, 79–124 (2020).

[26] van Delden, R. A. *et al.* Unidirectional molecular motor on a gold surface. *Nature* **437**, 1337–1340 (2005).

[27] Singhania, A., Kalita, S., Chettri, P. & Ghosh, S. Accounts of applied molecular rotors and rotary motors: recent advances. *Nanoscale Advances* **5**, 3177–3208 (2023).

[28] Ariga, K., Song, J. & Kawakami, K. Molecular machines working at interfaces: physics, chemistry, evolution and nanoarchitectonics. *Physical Chemistry Chemical Physics* **26**, 13532–13560 (2024).

[29] Yang, T. & Zhang, R. STM studies for surface-mounted molecular rotors: a mini review. *AAPPS Bulletin* **34**, 6 (2024).

[30] Barth, J. V. Molecular architectonic on metal surfaces. *Annual Review of Physical Chemistry* **58**, 375–407 (2007).

[31] Bartels, L. Tailoring molecular layers at metal surfaces. *Nature Chemistry* **2**, 87–95 (2010).

[32] Gao, W. *et al.* Determining the adsorption energies of small molecules with the intrinsic properties of adsorbates and substrates. *Nature Communications* **11** (2020).

[33] DeJong, M. *et al.* Small molecule binding to surface-supported single-site transition-metal reaction centres. *Nature Communications* **13**, 7407 (2022).

[34] Wojtecki, R. *et al.* Additive Lithography–Organic Monolayer Patterning Coupled with an Area-Selective Deposition. *ACS Applied Materials & Interfaces* **13**, 9081–9090 (2021).

[35] Singh, A., Shi, A. & Claridge, S. A. Nanometer-scale patterning of hard and soft interfaces: from photolithography to molecular-scale design. *Chemical Communications* **58**, 13059–13070 (2022).

[36] Pollard, M. M., Meetsma, A. & Feringa, B. L. A redesign of light-driven rotary molecular motors. *Organic and Biomolecular Chemistry* **6**, 507–512 (2008).

[37] Sheng, J. *et al.* Formylation boosts the performance of light-driven overcrowded alkene-derived rotary molecular motors. *Nature Chemistry* (2024).

[38] Dral, P. O., Wu, X. & Thiel, W. Semiempirical quantum-chemical methods with orthogonalization and dispersion corrections. *Journal of Chemical Theory and Computation* **15**, 1743–1760 (2019).

[39] Liu, F. & Morokuma, K. Computational study on the working mechanism of a stilbene light-driven molecular rotary motor: Sloped minimal energy path and unidirectional nonadiabatic photoisomerization. *Journal of the American Chemical Society* **134**, 4864–4876 (2012).

[40] Pang, X. *et al.* "Watching" the Dark State in Ultrafast Nonadiabatic Photoisomerization Process of a Light-Driven Molecular Rotary Motor. *The Journal of Physical Chemistry A* **121**, 1240–1249 (2017).

[41] Wilcken, R. *et al.* Complete Mechanism of Hemithioindigo Motor Rotation. *Journal of the American Chemical Society* **140**, 5311–5318 (2018).

[42] Filatov, M., Paolino, M., Min, S. K. & Choi, C. H. Design and photoisomerization dynamics of a new family of synthetic 2-stroke light driven molecular rotary motors. *Chemical Communications* **55**, 5247–5250 (2019).

[43] Filatov, M. Understanding the dynamics behind photoisomerization of light-driven molecular rotary motors. *WIREs Computational Molecular Science* **3**, 427–437 (2013).

[44] Conyard, J. *et al.* Ultrafast dynamics in the power stroke of a molecular rotary motor. *Nature Chemistry* **4**, 547–551 (2012).

[45] Kazaryan, A., Lan, Z., Schäfer, L. V., Thiel, W. & Filatov, M. Surface Hopping Excited-State Dynamics Study of the Photoisomerization of a Light-Driven Fluorene Molecular Rotary Motor. *Journal of Chemical Theory and Computation* **7**, 2189–2199 (2011).

[46] Filatov, M. *et al.* Towards the engineering of a photon-only two-stroke rotary molecular motor. *Nature Communications* **13**, 6433 (2022).

[47] Shaik, S., Danovich, D., Joy, J., Wang, Z. & Stuyver, T. Electric-Field Mediated Chemistry: Uncovering and Exploiting the Potential of (Oriented) Electric Fields to Exert Chemical

Catalysis and Reaction Control. *Journal of the American Chemical Society* **142**, 12551–12562 (2020).

[48] Li, S. Y. *et al.* Tri-Stable Structural Switching in 2D Molecular Assembly at the Liquid/Solid Interface Triggered by External Electric Field. *ACS Nano* **13**, 6751–6759 (2019).

[49] Frauhammer, T. *et al.* Addressing a lattice of rotatable molecular dipoles with the electric field of an STM tip. *Physical Chemistry Chemical Physics* **23**, 4874–4881 (2021).

[50] Zhang, Y. *et al.* Simultaneous and coordinated rotational switching of all molecular rotors in a network. *Nature Nanotechnology* **11**, 706–712 (2016).

[51] Conyard, J., Cnossen, A., Browne, W. R., Feringa, B. L. & Meech, S. R. Chemically Optimizing Operational Efficiency of Molecular Rotary Motors. *Journal of the American Chemical Society* **136**, 9692–9700 (2014).